

Simulation of symmetric nuclei and the role of Pauli potential in binding energies and radii

M. Ángeles Pérez-García ^{1 *}, K. Tsushima ^{2 †}, A. Valcarce ^{1 ‡}

¹*Departamento de Física Fundamental and Instituto
Universitario de Física Fundamental y Matemáticas,
IUFFyM, Universidad de Salamanca,
Plaza de la Merced s/n 37008 Salamanca*

²*Thomas Jefferson National Accelerator Facility 12000
Jefferson Avenue, Newport News, VA 23606, USA*

(Dated: March 17, 2008)

Abstract

It is shown that the use of a density dependent effective Pauli potential together with a nucleon-nucleon interaction potential plays a crucial role to reproduce not only the binding energies but also the matter root mean square radii of medium mass range spin-isospin saturated nuclei. This study is performed with a semiclassical Monte Carlo many-body simulation within the context of a simplified nucleon-nucleon interaction to focus on the effect of the genuine correlations due to the fermionic nature of nucleons. The procedure obtained is rather robust and it does not depend on the detailed features of the nucleon-nucleon interaction. For nuclei below saturation the density dependence may be represented in terms either of the nucleon number, A , or the associated Fermi momenta. When testing the simulation procedure for idealized "infinite" symmetric nuclear matter within the corresponding range of densities, it turns out that finite size effects affect the Pauli potential strength parametrization in systems up to about 120 particles while remaining approximately stable for larger systems.

PACS numbers: 07.05.Tp, 21.10.D, 21.65.+f

* mperezga@usal.es

† tsushima@jlab.org

‡ valcarce@usal.es

I. INTRODUCTION

We have recently demonstrated [1] that one can always expect to be able to reproduce the empirical binding energies for a set of nuclei by introducing a proper density dependent Pauli potential in terms of a single variable, the nucleon number A . Such a result is the consequence of a delicate counterbalance between kinetic and potential energetic contributions. A deeper understanding of the nuclear saturation mechanism and reproduction of other observables for nuclei has been made possible due to the richness of available nuclear data. Since the pioneering shell model calculations [2] and the so-called "Coester band" [3], many microscopic investigations have been devoted to study the properties of many-nucleon systems with a variety of approaches as *i.e.* relativistic mean fields [4], quark-based models [5, 6] and chiral dynamics [7]. On the other hand, studies based on computer simulations with Monte Carlo techniques and/or (quantum) molecular dynamics, have proved themselves to be very powerful to investigate many-nucleon systems such as subthreshold kaon production [8, 9] and multifragmentation [8, 10] in heavy ion collisions, and the *nuclear pasta* phase [11, 12, 13, 14]. Most of these works, based on semiclassical simulations, treat nuclei as composite objects interacting through effective potentials containing the essential features of the system. Especially, the effects of the Pauli principle, the basic quantum feature for many-fermion systems, is simulated by means of an effective potential depending on the position and momentum of the interacting nucleons. This was firstly suggested by Wilets *et al.* [15] in the context of classical many-body nuclear models. Later, approaches such as fermionic molecular dynamics (FMD) [16] and antisymmetrized molecular dynamics (AMD) [17], include the Pauli principle in a quantum mechanical manner. However, it is still not practical to apply these methods to study heavy nuclei and nuclear matter, due to the need of heavy computational calculation, and unestablished (anti)periodic boundary conditions to simulate an infinitely large nuclear system [18].

In this work we go a step further from our previous study [1] by considering a refined effective spin-dependent NN interaction and analyzing other nuclear properties for medium mass nuclei and heavy nuclear systems. We will firstly deduce a corresponding density dependent effective Pauli potential reproducing the empirical nuclear binding energies. For this purpose, without loss of generality, we will focus on medium mass range nuclei with $8 \leq A \leq 44$. It turns out that the spin dependence has only a very moderate impact,

with the relevant contributions coming from the in-medium effects of the effective Pauli potential. In addition, we will also evaluate the root mean square radius (rms) of spin-isospin saturated nuclei and their density distributions. When the simulation is extended for idealized infinite symmetric nuclear matter, it turns out that finite size affects the Pauli potential strength up to about 120 particles while remaining almost stable for larger systems. The picture arising from the present semiclassical simulation of nuclei, though simplified, accounts for basic properties of these systems. In the medium mass range nuclei, the density dependence could be either described in terms of the nucleon number or, as we will show, a function of the associated nucleus Fermi momentum. This treatment relates to that of recent approaches applied in chiral dynamics [7]. The present description can be considered, then, as an improvement of previous simulation work where neither antisymmetrization effects nor density dependence were considered. The derived effective Pauli potential does not depend on local densities as occurs, for example, in work using Skyrme models [8]. Nonetheless, even if not local, the density dependence in the effective Pauli potential becomes crucial to achieve saturation.

The structure of the paper is as follows. In section II, we describe the different nuclear potentials used in the simulations. First, we introduce S -wave NN interactions without spin nor isospin dependence. This makes easier to analyze the role of the Pauli potential and its nuclear density dependence. Next, we consider improved spin dependent NN interactions. Results will be presented in section III, and summary and conclusions will be given in section IV.

II. NUCLEAR INTERACTION MODELS

In this section we present the different simplified nuclear models which will be used in our simulations. We restrict ourselves to spin-isospin saturated, $Z = N$ (even Z and N) nuclei with mass number A in the range $8 \leq A \leq 44$. In addition, nucleons are treated as classical, structureless particles.

A. Square-well potential

First, we consider a NN interaction based on a square-well potential without any dependence on spin nor isospin. While the model is simple, it retains the basic features of the NN interaction, short-range repulsion and intermediate range attraction. The NN interaction potential between the i -th and j -th nucleons is given by,

$$V_{NN}(r_{ij}) = \begin{cases} V_{Core}, & \text{for } 0 \leq r_{ij} < a, \\ -V_0, & \text{for } a \leq r_{ij} < a + b, \\ 0, & \text{for } a + b \leq r_{ij}, \end{cases} \quad (1)$$

where $r_{ij} = |\mathbf{r}_i - \mathbf{r}_j|$ is their relative distance. This potential consists of a repulsive core of strength V_{Core} and width a , and an attractive well of depth V_0 and width b . We will consider values $V_{Core} = 100$ MeV, $V_0 = 3$ MeV, $a = 2$ fm and $b = 2$ fm. The core strength gives only a very moderate contribution to the binding energies (as easily deduced from the different values we may use [1]), only preventing nucleons from occupying the inner region in configuration space. However the spatial parameters, a and b , are crucial to reproduce satisfactorily matter root mean square radii as will be explained later in this section. The corresponding Hamiltonian is given by,

$$H = \sum_{i=1}^A \frac{\mathbf{p}_i^2}{2m_N} + \sum_{i=1, j>i}^A V_{NN}(r_{ij}), \quad (2)$$

where \mathbf{p}_i is the 3-momentum of i -th nucleon with mass m_N . From now on we will refer to this model as SW.

Next, we consider a refined NN interaction including the Coulomb potential:

$$V_{Coul}(r_{ij}) = \frac{e^2}{4\pi r_{ij}} (1/2 + \tau_i)(1/2 + \tau_j), \quad (3)$$

where τ_i (τ_j) is the isospin third-component of i -th (j -th) nucleon ($+1/2$ for protons, $-1/2$ for neutrons), and e is the proton electric charge. Then, the Hamiltonian is given by,

$$H = \sum_{i=1}^A \frac{\mathbf{p}_i^2}{2m_N} + \sum_{i=1, j>i}^A [V_{NN}(r_{ij}) + V_{Coul}(r_{ij})]. \quad (4)$$

We will refer to this model as SWC.

Since nucleons are fermions, they obey the Pauli principle. In the present treatment this is mimicked by introducing an effective potential, which prevents nucleons from occupying

the same phase space volume when they have the same quantum numbers. This was first suggested by Wilets *et al.* [15]. Later, a Gaussian form of the Pauli potential has been introduced by Dorso *et al.* [19]. In this way one can reproduce well kinetic energies per nucleon in a Fermi gas, although it fails to describe other basic features such as two-body correlation functions at low temperature [20]. Using this effective Pauli potential depending not only on the position but also on the momentum of the interacting fermions in a Hamiltonian approach, an effective nucleon mass which grows largely with increasing nucleon density arises. This results in very slow nucleons, and may lead to quasi-crystallized nuclear Fermi gases if not properly considered [21].

In this work we use the Pauli potential form proposed by Dorso *et al.* [19],

$$V_{Pauli}(r_{ij}, p_{ij}) = V_P \exp \left(-\frac{r_{ij}^2}{2q_0^2} - \frac{p_{ij}^2}{2p_0^2} \right) \delta_{\tau_i \tau_j} \delta_{\sigma_i \sigma_j}, \quad (5)$$

where $p_{ij} = |\mathbf{p}_i - \mathbf{p}_j|$ is the relative 3-momentum of the i -th and j -th nucleons, with $\delta_{\tau_i \tau_j}$ ($\delta_{\sigma_i \sigma_j}$) being the Kronecker's delta for the isospin (spin) third-component. We will differentiate two cases: (i) V_P , q_0 and p_0 are constant fixed to reproduce the empirical binding energy per nucleon ($-E/A$) of ^{16}O , 7.98 MeV [22], and (ii) allow them to be density dependent. The models corresponding to (i) and (ii), will be referred to as SWCPo and SWCP, respectively. In addition, in both cases, spatial parameters in Eq. (1) take the values $a = 2$ fm and $b = 2$ fm as they have been adjusted to reproduce the ^{16}O matter rms radius to 2.72 fm [23]. The Hamiltonian for these models, without specifying the density dependence for the Pauli potential, is given by:

$$H = \sum_{i=1}^A \frac{\mathbf{p}_i^2}{2m_N} + \sum_{i=1, j>i}^A [V_{NN}(r_{ij}) + V(r_{ij})_{Coul} + V_{Pauli}(r_{ij}, p_{ij})]. \quad (6)$$

To extract the density (Fermi momentum) dependence of q_0 and p_0 in the Pauli potential in Eq. (5), we use the Fermi momenta deduced in Ref. [24] from the quasielastic electron scattering on several nuclei, and interpolate for the nuclei studied later. Note that with this parametrization of the Pauli potential the more general local density dependence has been parametrized in terms of one single parameter based on a simplified Fermi gas picture.

In a nucleus, a typical nucleon sphere radius r may be given by,

$$r = \left(\frac{3}{4\pi\rho} \right)^{1/3}, \quad (7)$$

where $\rho = 2p_F^3/3\pi^2$ is the nucleon density and p_F the Fermi momentum of nucleons in the nucleus. Then, the averaged inter-nucleon distance $2r$ may be estimated as $(2r/\sqrt{2}q_0) \simeq 1$, where q_0 is an "effective range" of the Pauli potential. This leads to,

$$q_0 \simeq \frac{\hbar(9\pi)^{1/3}}{\sqrt{2}p_F}, \quad (8)$$

$$p_0 \simeq \frac{\hbar}{q_0} = \frac{\sqrt{2}}{(9\pi)^{1/3}}p_F, \quad (9)$$

with the uncertainty principle for q_0 and p_0 to satisfy $q_0 p_0 \simeq \hbar$.

As mentioned above, we will first consider a model where the Pauli potential parameters, V_P , q_0 , and p_0 are fixed to reproduce the binding energy of ^{16}O , what gives rise to $(V_P, q_0, p_0) = (41 \text{ MeV}, 1.88 \text{ fm}, 104.96 \text{ MeV/c})$. Secondly, we consider another parametrization of the Pauli potential allowing a density (p_F) dependence trying to reproduce the empirical binding energies for spin-isospin saturated nuclei, together with the relations in Eqs. (8) and (9). This leads to,

$$V_{Pauli}(r_{ij}, p_{ij}, p_F) = V_P(p_F) \exp \left[-\frac{r_{ij}^2}{2q_0^2(p_F)} - \frac{p_{ij}^2}{2p_0^2(p_F)} \right] \delta_{\tau_i \tau_j} \delta_{\sigma_i \sigma_j} \text{ (MeV)}. \quad (10)$$

It is worth noting that this approach has some similarities to what is used in other contexts, such as chiral dynamics [7]. This may imply that the variable p_F in Eq. (10), is appropriate to characterize the many-nucleon system.

B. Spin dependent square-well potential

The NN interaction potentials we have described so far may be more generally described by introducing spin dependence. Note that this also implies isospin dependence in order to satisfy the Pauli principle. We consider a simple potential for the spin parallel ($\uparrow\uparrow, \downarrow\downarrow$) and antiparallel ($\uparrow\downarrow, \downarrow\uparrow$) pairs of nucleons:

$$V_{NN}^{spins}(r_{ij}) = \begin{cases} V_{Core}, & \text{for } 0 \leq r_{ij} < a, \\ -V_0^{\uparrow\uparrow, \downarrow\downarrow} \delta_{\sigma_i \sigma_j} - V_0^{\uparrow\downarrow, \downarrow\uparrow} (1 - \delta_{\sigma_i \sigma_j}), & \text{for } a \leq r_{ij} < a + b, \\ 0, & \text{for } a + b \leq r_{ij}. \end{cases} \quad (11)$$

We distinguish three different possibilities for the strength of each spin dependent term:

(i) Model SD1, where the spin parallel potential is more attractive than the antiparallel, $|V_0^{\uparrow\uparrow, \downarrow\downarrow}| > |V_0^{\uparrow\downarrow, \downarrow\uparrow}|$; (ii) Model SD2, the opposite case, $|V_0^{\uparrow\uparrow, \downarrow\downarrow}| < |V_0^{\uparrow\downarrow, \downarrow\uparrow}|$; (iii) Model SD3, for

the case, $|V_0^{\uparrow\uparrow,\downarrow\downarrow}| = |V_0^{\uparrow\downarrow,\downarrow\uparrow}|$. We will consider values $a = 1$ fm and $b = 2$ fm, different from those used for the models described in Sect. II A. In this way we introduce some dependence on the spatial parameter value a in Eq. (1). We have verified that parameter a (and also b) is mainly responsible for reproducing rms radii but has a very moderate impact on binding energies. We will mainly focus on the effect of the spin dependence on binding energies. The different balance between the parallel and antiparallel strengths will allow us to overcome the possible consequences of the simplification including only S -wave interactions. Inclusion of also the D -wave interactions, which only couple to the 3S_1 channel (in the present case, e.g., the interaction between $(p \uparrow) - (n \uparrow)$ pair) would modify the balance between the attraction in the spin parallel and antiparallel cases.

Finally, let us mention that although we have not considered a possible radial dependence on the interactions, in the case of binding energies will not have observable effects. The strength of $V_0^{\uparrow\uparrow,\downarrow\downarrow}$ and $V_0^{\uparrow\downarrow,\downarrow\uparrow}$ for the SD1, SD2 and SD3 models are chosen rather arbitrarily but they all reproduce the empirical value, $-E/A = 7.98$ MeV of ^{16}O , together with the same Pauli potential in the SWCPo model. The Hamiltonian for these models is given by:

$$H = \sum_{i=1}^A \frac{\mathbf{p}_i^2}{2m_N} + \sum_{i=1, j>i}^A \left[V_{NN}^{spins}(r_{ij}) + V_{Pauli}(r_{ij}, p_{ij}) + V_{Coul}(r_{ij}) \right]. \quad (12)$$

In Table I we summarize the strength of $V_0^{\uparrow\uparrow,\downarrow\downarrow}$ and $V_0^{\uparrow\downarrow,\downarrow\uparrow}$ for all models.

TABLE I: Strength (in MeV) of $V_0^{\uparrow\uparrow,\downarrow\downarrow}$ and $V_0^{\uparrow\downarrow,\downarrow\uparrow}$ for the SD1, SD2 and SD3 models.

Model	V_{Core}	$V_0^{\uparrow\uparrow,\downarrow\downarrow}$	$V_0^{\uparrow\downarrow,\downarrow\uparrow}$
SD1	100	5.8	0.5
SD2	100	0.5	5
SD3	100	3	3

III. SIMULATION RESULTS

In this section we present the results obtained using Monte Carlo simulations of the nuclear systems where a typical value for low temperature, $T = 1$ MeV, is adopted. Initially, the nucleons are uniformly distributed inside a sphere of radius R_0 , within a cubic box of

volume $V = L^3$ and impose $L \gg r_{ij}$. Up to $R_0 \simeq 5$ fm the binding energy per nucleon has rather stable values, although it tends to vanish rapidly for larger R_0 . This reflects the fact that for large values of R_0 some nucleons would not feel any attraction (see Eq. (1)). Then, using the Metropolis algorithm [25], the initial random seed is iterated until the energetic configuration achieves the lowest possible value. In addition, we must check that a clustered configuration of nucleons is indeed formed, a nucleus. Once the system is thermalized after performing a sufficiently large number (several thousands) of Monte Carlo sweeps, we take data to calculate the statistical average for thermodynamic quantities such as kinetic and potential energies and root mean square radii.

First, we discuss the results of the SWCPo model introduced in Sect. II A, based on the density independent Pauli potential fixed to reproduce the binding energy per nucleon and matter rms radius of ^{16}O .

In Fig. 1 we show the SWCPo results for $-E/A$ by the solid line compared to empirical values [22] (crosses).

As can be seen, using the density independent Pauli potential, $-E/A$ grows linearly as the nucleon number increases. Thus, the empirically observed saturation for $-E/A$ cannot be achieved.

Let us now discuss the results for the SWCP model, with the density dependent Pauli potential. Before presenting the results for $-E/A$, we show in Fig. 2 the p_F for V_P obtained to reproduce the empirical $-E/A$ values for the spin-isospin saturated nuclei. The strength $V_P(p_F)$ increases as Fermi momentum (density) increases. The strength obtained for each nuclear species can be mapped as a function of the Fermi momentum extracted from the quasielastic electron scattering off nuclei [24]. This behavior is analogous to the vector mean field in Hartree approximation in relativistic mean field models [4].

We show in Fig. 3 the results for $-E/A$ obtained in the SWCP model with the use of the density dependent Pauli potential, Eq. (10). The statistical uncertainty of these calculated values is at most 5 %.

In Fig. 4 we show the matter rms radius (boxes) as a function of mass number, A , for a set of nuclei as calculated with the density dependent fit in Eq. (10). We can see that they approximately follow the liquid drop model results (dashed line) given by the $R = r_0 A^{1/3}$ with $r_0 \approx 1.1 \text{ fm}$.

In Figs. 5 and 6 we show the density distribution calculated for an ^{16}O nucleus and a

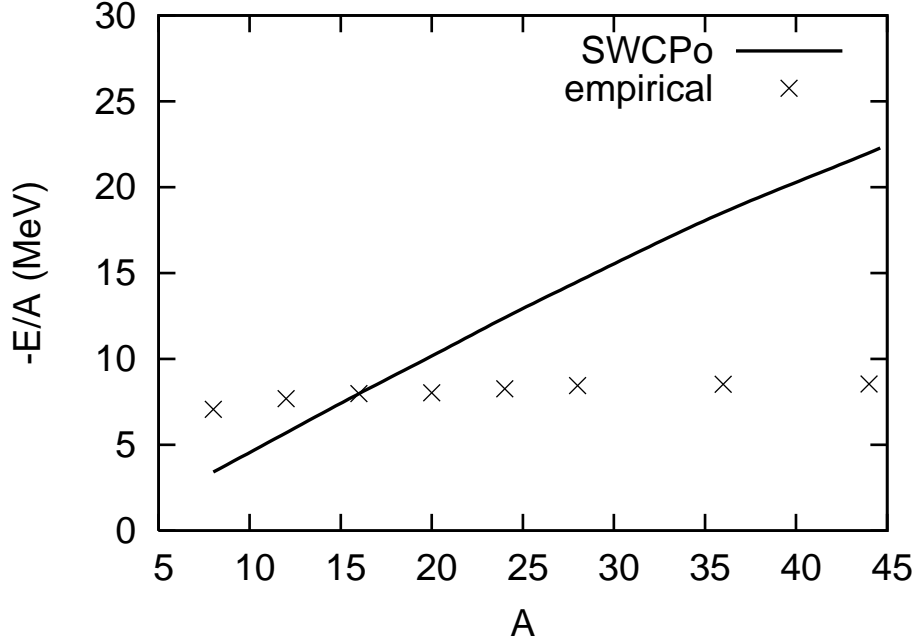


FIG. 1: Binding energy per nucleon, $-E/A$, calculated in the SWCPo model. Empirical data, shown by crosses, are taken from Ref. [22] for even nuclei. We have calculated nuclei with $A = 8, 12, 16, \dots, 44$ and the solid line goes through all calculated points, being only valid for these even nuclei. This will also apply to the other figures along the text.

^{20}Ne nucleus, respectively. We can see that most of the mass is located in the nuclear central region. The decrease of particle population at small distances is due to the strong repulsive core of the interaction used. We have fit this distribution to a typical Woods-Saxon form $\rho(r) = \frac{\beta}{1+e^{(r-\alpha)/\gamma}}$ obtaining a set of values for ^{16}O , $\beta = 0.066 \pm 0.002 fm^{-3}$, $\alpha = 4.0 \pm 0.5 fm$ and $\gamma = 0.41 \pm 0.45 fm$ and for ^{20}Ne we get $\beta = 0.068 \pm 0.007 fm^{-3}$, $\alpha = 3.97 \pm 0.20 fm$ and $\gamma = 0.1 \pm 0.5 fm$ which are in reasonable agreement with those of mean field calculations [4]. Note that the value α indicates where the central density remains approximately constant, while the matter rms radius gets contribution also from the more extended spatial region of nucleons in the nucleus. It is worth noting that the values of the parameter a and b are mainly responsible for reproducing the rms radii in this approach.

Next, we present in Fig. 7 the comparison for the binding energy per nucleon obtained with the different models described in Sect. II A. The solid (long-dashed) [short-dashed] line shows the SW (SWC) [SWCP] model. Both, the SW and SWC models, cannot achieve

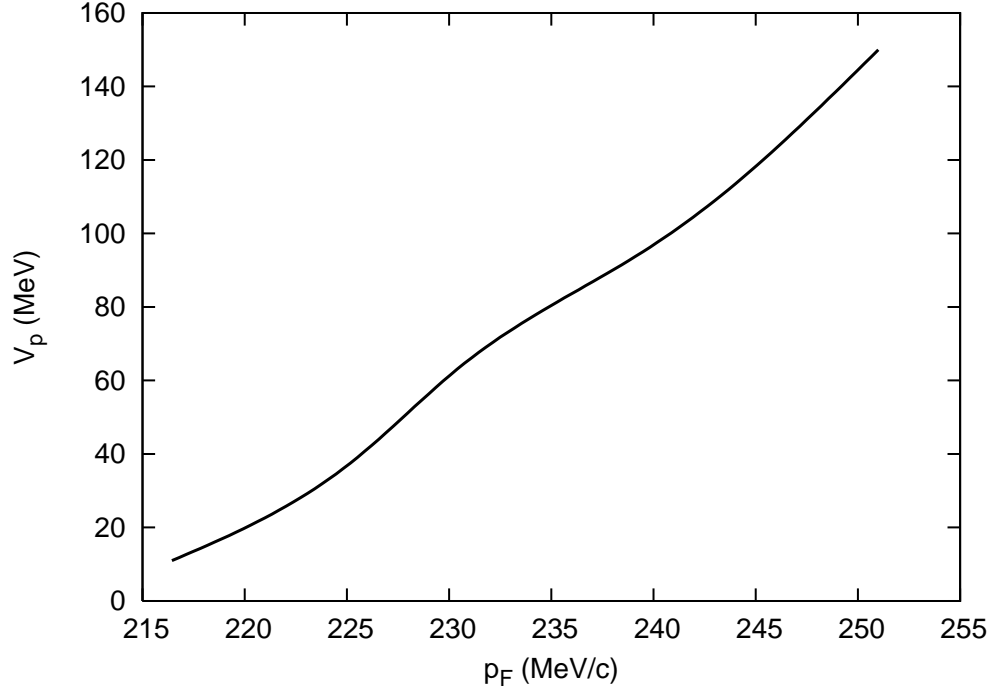


FIG. 2: Pauli potential strength V_P as a function of the Fermi momentum, p_F .

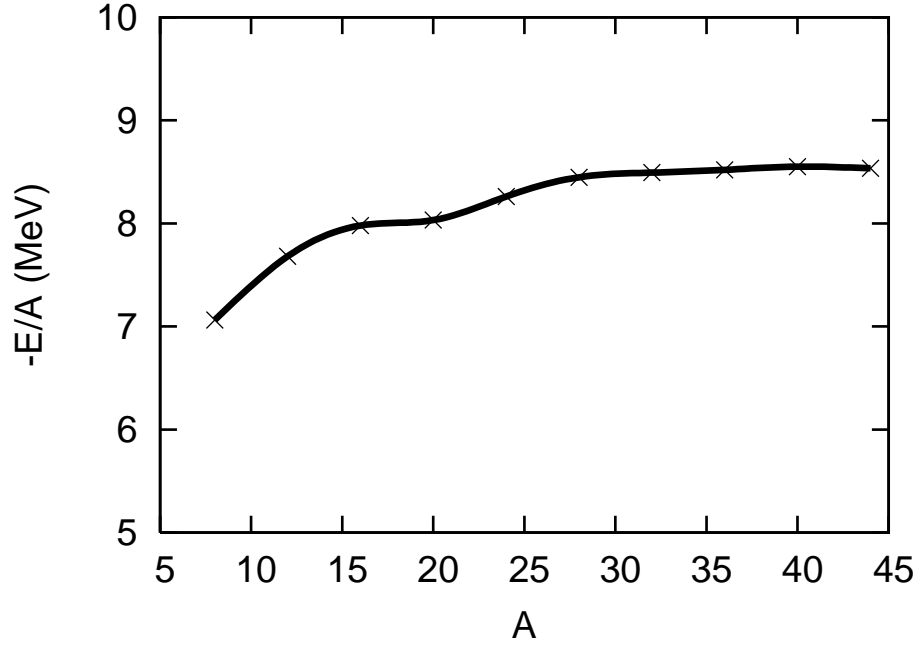


FIG. 3: Binding energy per nucleon for spin-isospin saturated nuclei for the SWCP model.

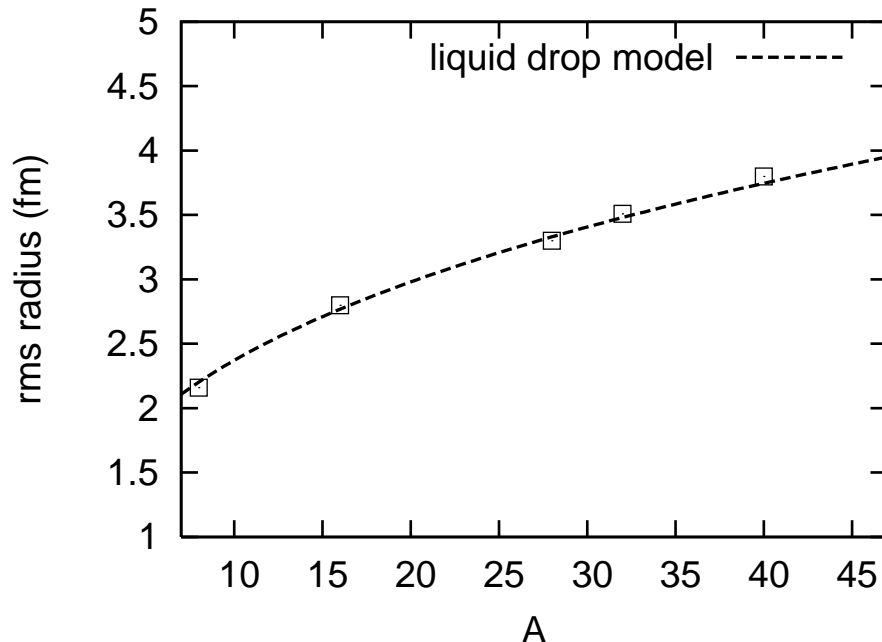


FIG. 4: Matter root mean square radius calculated as a function of mass number A for several nuclei using the SWCP model. See details in the text. Liquid drop model calculation is shown for comparison.

the saturation for $-E/A$. The Coulomb potential can negligibly help to achieve $-E/A$ saturation as expected, although it is important for some properties of finite nuclei [4].

In order to understand how the energy saturation is obtained in the SWCP model, we draw separately in Fig. 8 the contribution of the kinetic energy per nucleon K/A (dashed line), and potential energy per nucleon V/A (short-dashed line) together with E/A (solid line). We see the kinetic energy per nucleon largely deviates from the classical value, $K/A = (3/2)k_B T$, (i.e. $K/A = 1.5$ MeV in the present case with $T = 1$ MeV) due to the contribution of the density dependent Pauli potential. Thus, this shows that the kinetic and canonical momenta are completely different as the nucleon density increases [21]. A balance between the large potential and kinetic energy contribution leads to $-E/A$ saturation. This cancellation arises as a consequence of the increasing kinetic contribution of Pauli correlations [1]. This may be analogous to the mechanism of saturation in relativistic mean field models which involves the cancellation between the attractive scalar and the repulsive vector potentials [4].

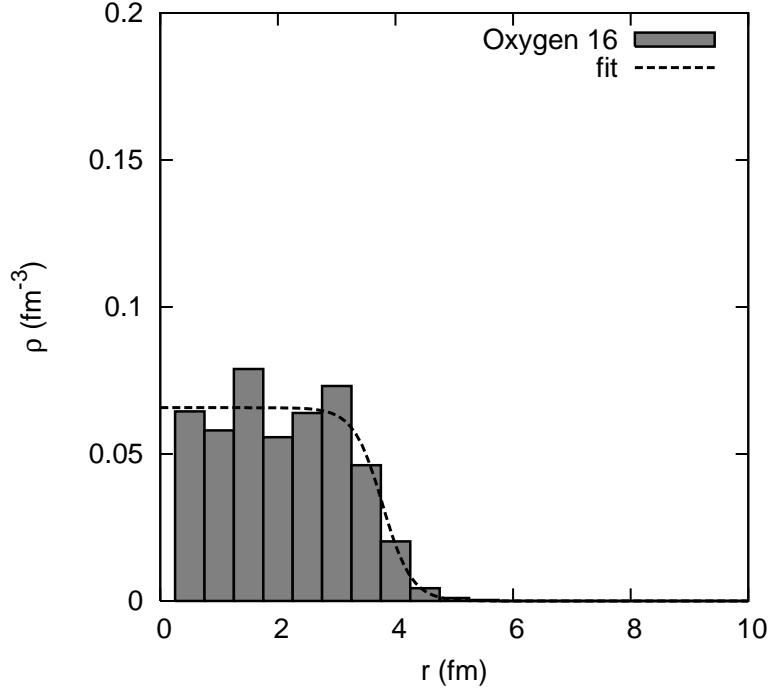


FIG. 5: ^{16}O density distribution histogram as given by the SWCP model. Dashed line shows the Woods-Saxon fit for this nucleus. See details in the text.

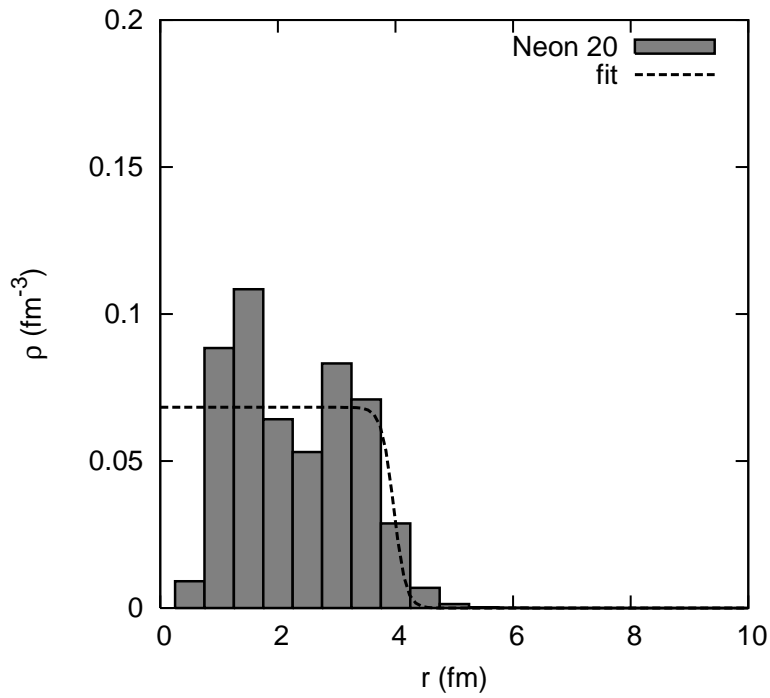


FIG. 6: Same as Fig. 5 for ^{20}Ne .

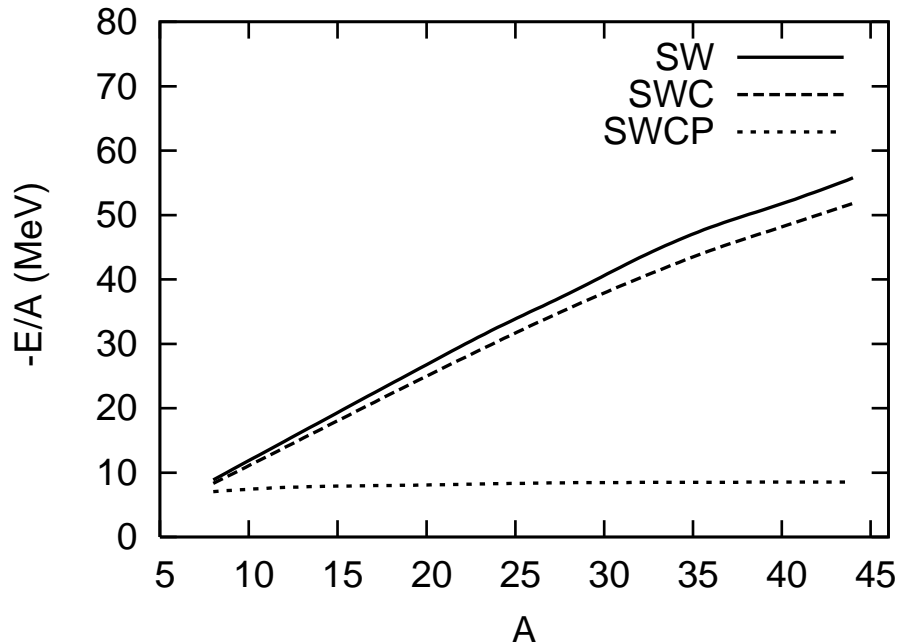


FIG. 7: Binding energy per nucleon ($-E/A$) for different NN interaction models.

Let us now study the effect of spin dependent potentials, using the SD1, SD2 and SD3 models described in Sect. II B. In this case we will work with the density independent Pauli potential described in Sect. II A, in order to see the effect of spin-dependent forces in the energy saturation. The results are shown in Fig. 9. The solid (long-dashed) [short-dashed] line stands for the results of the SD1 (SD2) [SD3] model, together with the empirical data (crosses) [22]. We can see again the $-E/A$ saturation cannot be obtained even using an improved spin dependent NN potential.

In Fig. 10 we show energy per nucleon for the ideal "infinite" symmetric nuclear matter (SNM) case at $T = 0$ MeV (solid line). An incompressibility value of $K \approx 230$ MeV has been assumed and $\rho_0 = 0.165 fm^{-3}$. Correspondingly the range in densities or Fermi momentum can be extracted as done in ref.[24] as $\rho = \frac{2p_F^3}{3\pi^2}$ for the set of symmetric spin saturated nuclei $8 \leq A \leq 44$ (dashed line). The lower and upper bounds in the density interval correspond to $\rho/\rho_0 = 0.51$ and $\rho/\rho_0 = 0.8$ respectively.

We now compare some results from heavier nuclear systems than the medium mass range nuclei considered in the previous sections in this work. In Fig. 11 we show the Pauli potential strength, V_P as a function of the particle number, A , for an idealized case of SNM, through the simulation for densities $\rho/\rho_0 = 0.58$ (solid line) and $\rho/\rho_0 = 0.7$ (dashed line). We can

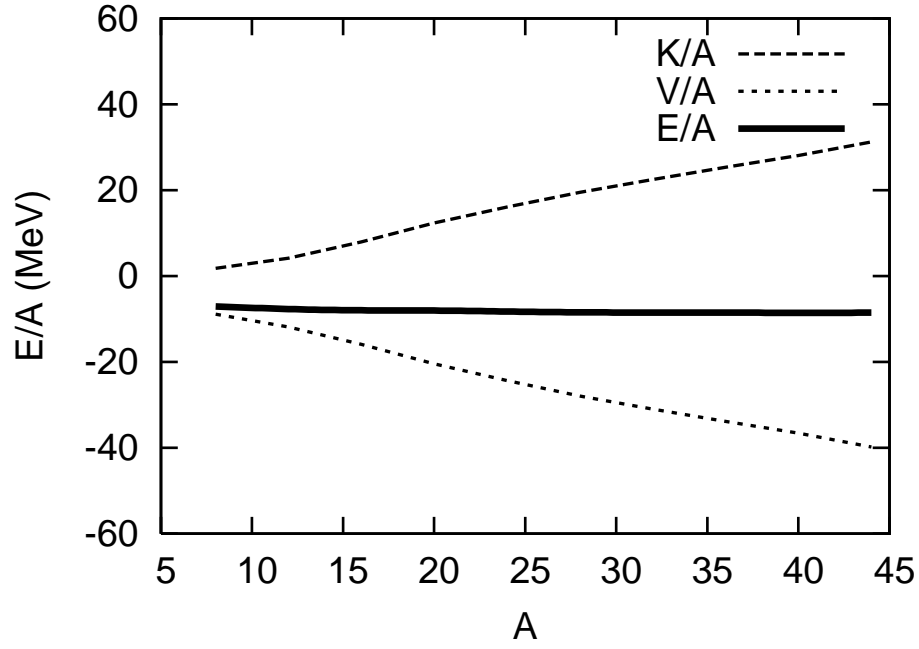


FIG. 8: Kinetic (K/A) and potential (V/A) energy per nucleon contributions to E/A .

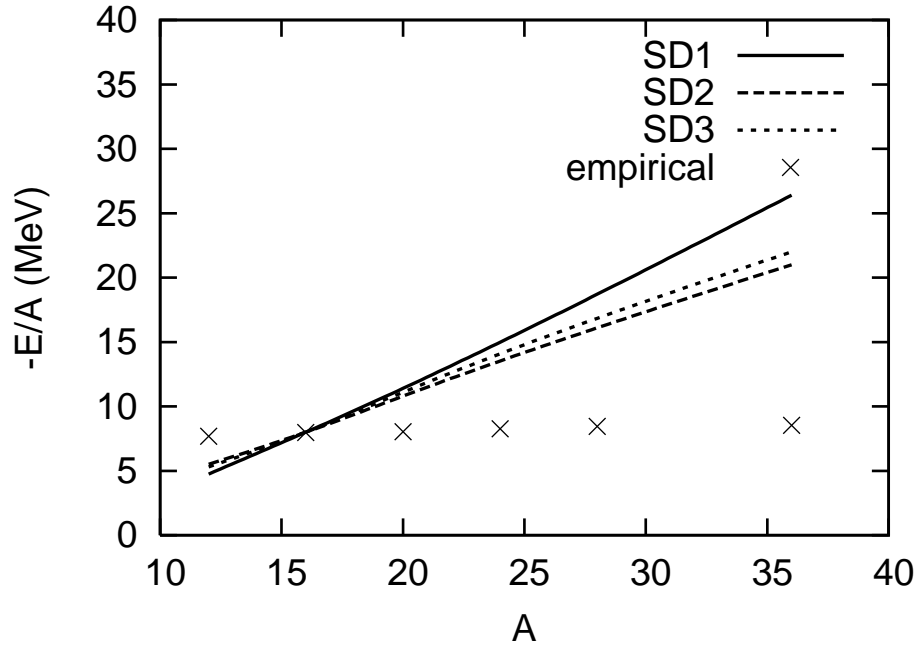


FIG. 9: Same as Fig. 2 for the SD1, SD2 and SD3 models.

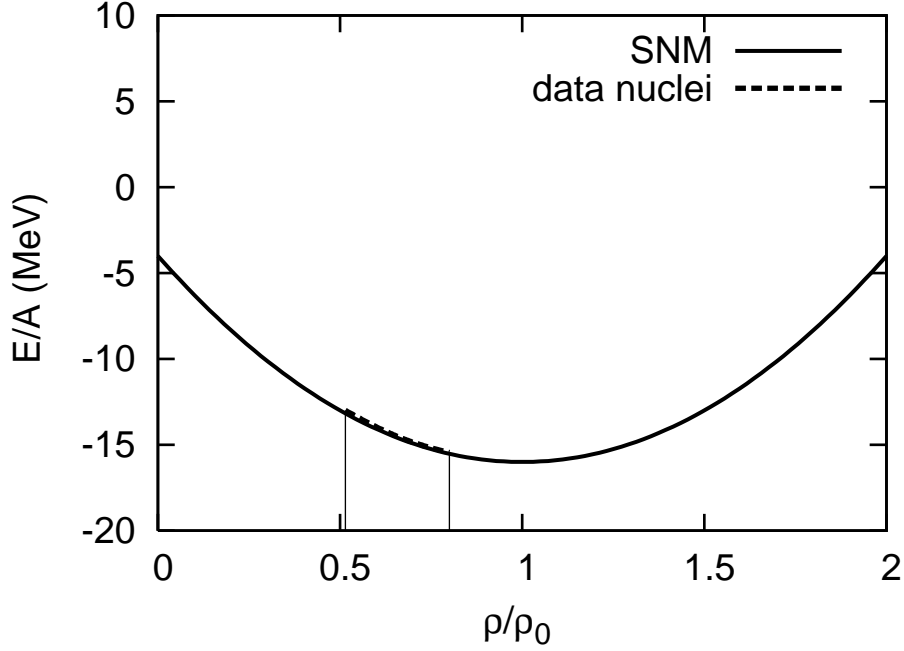


FIG. 10: Energy per particle in SNM at $T = 0$ and range in densities corresponding to the Fermi momentum of nuclei considered in this work. The lower bound in the density interval corresponds to $\rho/\rho_0 = 0.51$ and the upper to $\rho/\rho_0 = 0.8$.

see that finite size effects (particle number) are important up to values about $A \approx 120$ where the Pauli potential strength stabilize to an approximately constant value. The larger values for small A do not match those of finite nuclei since in this case nucleons are artificially constrained in a cube of length $L = (A/\rho)^{1/3}$. We use periodic boundary conditions as usual to minimize boundary effects near the walls of the simulation box. It is worth mentioning that as we consider heavier nuclei [1] the density dependence parametrized by the Fermi momentum must be replaced by the system size, A , since one can map out Pauli potential strengths in a clearly defined way. In Fig. 12 we show a thermalized configuration of a simulation of a SNM plasma at $T = 1$ MeV at a density $\rho/\rho_0 = 0.7$. In this homogeneous system of $A = 200$ particles, protons are shown as small dots while neutrons correspond to larger dots.

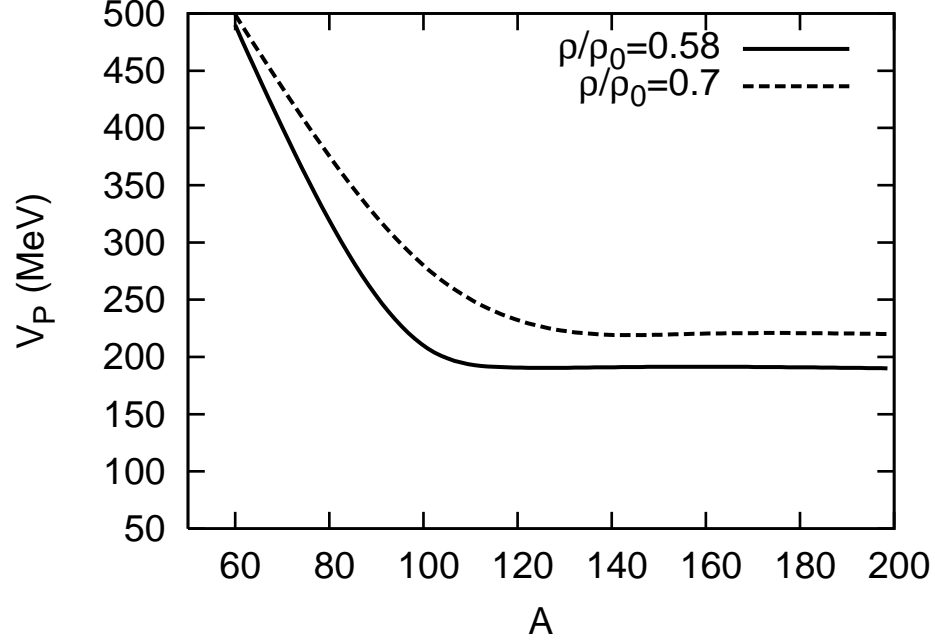


FIG. 11: Pauli potential strength as a function of the simulation system particle number for SNM for densities $\rho/\rho_0 = 0.58$ and $\rho/\rho_0 = 0.7$.

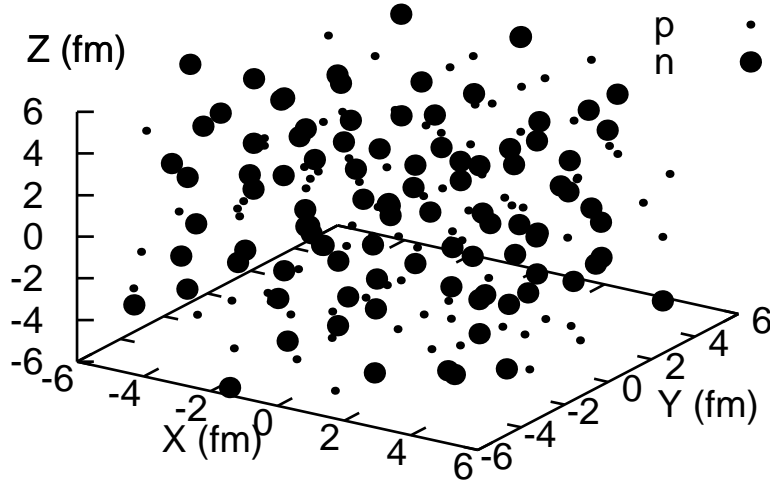


FIG. 12: Simulation box for a system of SNM consisting of 200 particles at a density $\rho/\rho_0 = 0.7$ and $T = 1$ MeV. Protons and neutrons are depicted with small and larger dots respectively.

IV. SUMMARY AND CONCLUSIONS

Using many-body simulations with Monte Carlo techniques we have pursued the study of an effective Pauli potential in the nuclear binding energy and matter rms radius considering density dependence. The density dependent effective Pauli potential partially simulates the effect of genuine fermionic correlations on semiclassical descriptions. For medium mass range nuclei with $8 \leq A \leq 44$ the nucleon number dependence into the effective Pauli potential can be replaced in terms of the Fermi momentum of the constituent nucleons. Even if spin dependent effects are explicitly included in the NN potential, an appropriate parametrization of the density dependence can still be derived in terms of the Fermi momentum. The density dependence in the effective Pauli potential is crucial to reproduce nuclear binding energy saturation, which is achieved by a balance of density dependent attractive and repulsive contributions in an analogous way to the relativistic mean field approach. Although for medium mass nuclei the density dependence can be described in terms of the Fermi momenta, the treatment of heavier nuclei requires to consider the density dependence in terms of the nucleon number, due to saturation of the Fermi momenta around 270 MeV/c.

The use of spin-isospin dependent NN potentials turns out to give only a moderate improvement for the binding energy per nucleon, but it is unable to achieve energy saturation unless a density dependent Pauli potential is used. Our results show that, provided a different set of values for the spatial parameters, a and b or potential well strength, V_0 , in the NN potential, a p_F dependent Pauli potential strength can always be parametrized to reproduce the empirical nuclear binding energies. The procedure presented in this work is robust. Then, each set of nuclei modelled by a given NN potential and calibrated by the empirical binding energies, can be tested by studying further properties of nuclei like, for example, when introducing some hyperonic content.

We have shown that, in the density range close to the saturation of nuclear binding energies, and for an idealized SNM system the Pauli potential strength depends on the size of the system and stabilizes to an approximately constant value around $A \approx 120$. The matter rms radii of medium mass range nuclei can be satisfactorily reproduced by tuning the spatial parameters of the NN interaction to a reference nucleus (in this work taken to be ^{16}O). A close agreement with the typical sizes of nuclei expected from a liquid drop model is obtained.

To summarize, the present approach may provide a practical efficient way to model a set of spin-isospin symmetric nuclei calibrated by the empirical binding energies and matter rms radii. It also can be regarded as a preliminary step for studying further properties of symmetric many-nucleon systems in semiclassical simulations. It is necessary to provide further insight into semiclassical effective potential models to study whether asymmetric systems can be treated in a similar fashion.

Acknowledgments

We would like to thank Tomoyuki Maruyama and A.W. Thomas for helpful discussions. M.A.P.G. would like to dedicate this work to the memory of J.M.L.G. This work has been partially funded by the Spanish Ministry of Education and Science projects DGI-FIS2006-05319, SAB2005-0059 and FPA2007-65748, and by Junta de Castilla y León under contracts SA-104104 and SA016A07. This work has been supported by the Spanish Consolider-Ingenio 2010 Programme CPAN (CSD2007-00042).

-
- [1] M.A. Pérez-García, K. Tsushima, and A. Valcarce, *Physics Letters B* **660** (2008) 600.
 - [2] For a review, B. A. Brown and B. H. Wildenthal, *Ann. Rev. Nucl. Part. Sci.* **38** (1988) 29.
 - [3] F. Coester, S. Cohen, B. Day, and C. M. Vincent, *Phys. Rev. C* **1** (1970) 769;
B. D. Day and F. Coester, *Phys. Rev. C* **13** (1976) 1720.
 - [4] B. D. Serot and J. D. Walecka, *Adv. Nucl. Phys.* **16** (1986) 1.
 - [5] P. A. M. Guichon, *Phys. Lett. B* **200** (1988) 235;
For a review, K. Saito, K. Tsushima and A. W. Thomas, *Prog. Part. Nucl. Phys.* **58** (2007) 1.
 - [6] For a review, Y. Fujiwara, Y. Suzuki and C. Nakamoto, *Prog. Part. Nucl. Phys.* **58** (2007) 439.
 - [7] N. Kaiser, S. Fritsch and W. Weise, *Nucl. Phys. A* **697** (2002) 255; *ibid A* **700** (2002) 343;
ibid A **724** (2003) 47;
S. Fritsch, N. Kaiser and W. Weise, *Nucl. Phys. A* **750** (2005) 259;
P. Finelli, N. Kaiser, D. Vretenar and W. Weise, *Nucl. Phys. A* **770** (2006) 1.
 - [8] J. Aichelin, *Phys. Rep.* **202** (1991) 233, and references therein; G. Peilert, J. Randrup, H. Stocker, and W. Greiner, *Phys. Lett. B* **260** (1991) 271; K. Niita *et al.*, *Phys. Rev. C* **52** (1995) 2620.

- [9] J. Aichelin and C.M. Ko, Phys. Rev. Lett. **55** (1985) 2661; G.E. Brown, C.M. Ko, Z.G. Wu, and L.H. Xia, Phys. Rev. C **43** (1991) 1881; G.Q. Li, C.-H. Lee, and G.E. Brown, Phys. Rev. Lett. **79** (1997) 5214; E.L. Bratkovskaya, W. Cassing, and U. Moesel, Nucl. Phys. A **622** (1997) 593; C. Fuchs, Prog. Part. Nucl. Phys. **56** (2006) 1.
- [10] G. Peilert, H. Stöcker, and W. G. Greiner, Phys. Rev. C **39** (1989) 1402; A. Ono, H. Horiuchi, T. Maruyama, and A. Ohnishi, Phys. Rev. Lett. **68** (1992) 2898; M. D. Partlan *et al.*, Phys. Rev. Lett. **75** (1995) 2100.
- [11] D. G. Ravenhall, C. J. Pethick, and J. R. Wilson, Phys. Rev. Lett. **50** (1983) 2066; M. Hashimoto, H. Seki, and M. Yamada, Prog. Theor. Phys. **71** (1984) 320.
- [12] G. Watanabe *et al.*, Phys. Rev. Lett. **94** (2005) 031101; G. Watanabe and H. Sonoda, arXiv:cond-mat.soft/0502515.
- [13] Toshiki Maruyama *et al.*, Phys. Rev. C **72** (2005) 015802.
- [14] C.J. Horowitz, M.A. Pérez-García, and J. Piekarewicz, Phys. Rev. C **69** (2004) 045804; C.J. Horowitz, M. A. Pérez-García, J. Carriere, D. K. Berry, and J. Piekarewicz, Phys. Rev. C **70** (2004) 065806.
- [15] L. Wilets, E. M. Henley, M. Kraft, and A. D. Mackellar, Nucl. Phys. **A282** (1977) 341; L. Wilets, Y. Yariv, and R. Chestnut, Nucl. Phys. A **301** (1978) 359.
- [16] H. Feldmeier, Nucl. Phys. A **515** (1990) 147.
- [17] A. Ono, H. Horiuchi, Toshiki Maruyama, and A. Ohnishi, Prog. Theor. Phys. **87** (1992) 1185.
- [18] Tomoyuki Maruyama, private communication.
- [19] C. Dorso, S. Duarte, and J. Randrup, Phys. Lett. B **188** (1987) 289; *ibid.* B **215** (1988) 611.
- [20] J. J. Neumann and G. I. Fai, Phys. Lett. B **329** (1994) 419.
- [21] J. Taruna, J. Piekarewicz and M. A. Pérez-García, J. Phys. A: Math. Theor. **41** (2008) 035308
- [22] G. Audi, A. H. Wapstra, and C. Thibault, Nucl. Phys. A **729** (2003) 337.
- [23] G. S. Anagnostatos, Int. J. Mod. Phys. E, **5** (1996) 557.
- [24] E. J. Moniz *et al.*, Phys. Rev. Lett. **26** (1971) 445.
- [25] M. Metropolis *et al.*, J. Chem. Phys. **21** (1953) 1087.